# Evaluation of Evaporative Cooling Chamber Using Computational Fluid Dynamics

George P. Fayiah-Tumbay, Duncan O. Mbuge, Urbanus N. Mutwiwa

***Abstract*----** Global temperatures are affecting almost all aspects of our society, including food security. A rise in temperature leads to a decrease in relative humidity. In Kenya, about 25–45% of fruits and vegetables perished because of inappropriate storage facilities. This is especially worrying among rural farmers. The primary objectives of this study were to evaluate the performance of the pumice evaporative cooling chamber with energy savings and thermal control and to simulate the storage chamber using a Computational Fluid Dynamics (CFD) model to predict storage temperature. A pumice evaporative cooling chamber of 14.58 m3 capacity, powered by solar energy, was designed and constructed at Jomo Kenyatta University of Agriculture and Technology for the study. Temperature, relative humidity, solar radiation, and wind speed were measured for natural convection, forced convection, evaporative, evapotranspiration, and combined cooling systems. The evaporative cooling data was used to develop a CFD model to predict the storage temperature. The three-dimensional CFD geometry was developed and used to simulate the cooling chamber with the Shear-Stress Transport (SST) k-omega model. The result was compared to experimental data and showed that, with no artificial influence on the cooler, the difference between ambient and storage temperature was 11.47 $^{O}$C, and the ambient and storage relative humidity was 42.44%. The cooling pad was 83% efficient. The ambient and storage temperature difference was 13.64 $^{O}$C, and humidity increased by 64.44% and 98.6%, respectively, for evaporative cooling. The CFD model predicted result was compared against experimental data with a 98% confidence for evaporative cooling and there was no significant difference. The study provided valuable guidelines for the design of an evaporative cooling system with efficient energy savings for the storage of fruits and vegetables.

***Keywords***: Computational fluid dynamics,modelling, Evaporative cooling, Postharvest loss

## I. INTRODUCTION

Post-harvest losses occur throughout the supply chain due to inappropriate storage facilities and market constraints that relate to fruit and vegetable storage. Rosegrant et al. [1] projected postharvest losses of fruits and vegetables at 25–50% of total production in regions with poor infrastructural development. These losses include mechanical damage, loss in nutritional value, and physiological and microbiological deterioration. Estimates of horticultural losses in Kenya have been reported to be as high as 50 percent [2], [3], [4]. Therefore, there is a pressing need for appropriate postharvest technologies in order to mitigate some of these losses.

Evaporation is the process by which water changes from liquid to gas or vapor. It is a process that serves as a pathway for water to move from the liquid state back into the water cycle. Evaporation can lead to a decrease in temperature and an increase in relative humidity. In its natural form, evaporation is considered one of the most economical methods used for cooling a given space [5]. The evaporation process is broadly classified into direct or indirect, and sometimes a combination of the two with other cooling cycles [6], [7]. Evaporative cooling is an energy-efficient alternative to refrigeration and compressor cooling [8].

Tremendous efforts have been made by several researchers towards the development of storage chambers. Roy and Pal [9] designed a low-cost evaporative cooler using locally available materials and reported a rise in relative humidity of 90% and above with a decrease in temperature of 10–15 ºC in the given space. Mordi and Olorunda [10] conducted a study on an evaporative cooling chamber for tomato storage and reported that the storage temperature was reduced by 8.2 C and relative humidity increased by 36.6%; thereby increasing the tomato shelf life by seven days. Kitinoja [11] found that evaporative cooling technology was capable of reducing the temperature in hot and dry climates by 25 ºC and enabling humidity levels of 90% in the surroundings. Manyozo et al. [12] investigated the effectiveness and performance of evaporative cooling chambers for tomato storage in Malawi during the rainy season and dry season using a charcoal cooler, brick cooler, and pot-in-pot cooler. They reported better results in all cases during the dry season as the shelf life of the stored tomatoes was increased by twenty-four days. They reported that, unlike mechanical refrigeration systems, an evaporative cooler is simple to operate and efficient in output. It saves energy in that it is only required for the fan and water pump and, in some instances, not at all [13].

The branch of fluid mechanics that utilizes computers and numerical methods to analyze and solve problems relating to fluid flow is called computational fluid dynamics (CFD). CFD models are computer-aided techniques used in industry to solve fluid problems by the application of general transport equations over a controlled volume [14]. Although modeling is often applied in mechanical cooling, some studies point to the use of models for evaporative cooling [15], [16], [17], [18]. Models are valuable tools for solving problems of fluid flow in storage chambers and are vital in the industry due to the complex nature of industrial fluid flow and problems of transport [15]. In practice, CFD is perfect in the elimination of

George P. Fayiah-Tumbay, Department of Environmental and Biosystems Engineering, UON, Nairobi, Kenya. +231777126660/+231886346464, Email: gpft2013@gmail.com

Eng. Dr. Duncan O. Mbuge. Department of Environmental and Biosystems Engineering, UON, Nairobi, Kenya

Prof. Urbanus N. Mutwiwa. Department of Agricultural and Biosystems Engineering, JKUAT, Nairobi, Kenya

competing design configurations, not a substitute for experimentation but a wonderful addition to problem-solving.

CFD has been used by many researchers to show its potential for analyzing fluid flow and heat transfer problems. Sohani et al. [15] used CFD to analyze the velocity and temperature distribution in an evaporative cooling system. Their analysis, however, did not address the issues of relative humidity and mass flow rate concerning the storage of fruits and vegetables. Luo et al. [16] developed a neural network that predicted the performance of an evaporative cooler for different operational situations. Montariza et al., [17] did a study on an evaporative cooling chamber with a water spray system using the Lagrangian-Eulerian approach in CFD. Their systematic approach allowed them to analyze several key factors associated with nozzle configuration, such as inlet relative humidity ratio, inlet air temperature, inlet air velocity, inlet water temperature, and inlet water droplet size. Although they validated these physical parameters against experimental data using CFD, their analysis was only applied to selected boundary conditions. Yanhua et al. [18] performed a numerical simulation to investigate fluid flow and heat transfer in a zero-energy evaporative cooler. They reported that a chamber size of 0.6 m, a filter size of 0.075 m, and a load of 30 kg led to an acceptable decrease in temperature with a corresponding increase in relative humidity. The numerical results were similar to experimental data, and they concluded that numerical simulation can be applied in an evaporative cooling chamber to predict the distribution of velocity, temperature, and relative humidity.

Miahra and Aharwal [19] conducted a review on the selection of turbulence models for CFD analysis of airflow and various aspects of the models for their application within cold storage. CFD models turbulent flow through any of the three turbulence models: Direct Numerical Simulation (DNS), Large Eddy Simulation (LES) or Detached Eddy Simulation (DES), and Reynolds–Averaged Navier–Stokes (RANS). However, DNS, LES, and DES provided results that were similar to experimental values but required lots of skills, time, and large computational capacity. They concluded that due to these challenges, most of the authors chose the RNS model for cold storage simulation. Finally, their finding was that RANS eddy viscosity models with a two-equation turbulence model and a three-dimensional geometry for modeling are capable of predicting airflow in a well-designed and constructed cold storage chamber. Adarsh and Jinu [20] designed a control mechanism for an evaporative cooling system to regulate the greenhouse cooling system. The system was able to control the amount of air volume flow rate in a fan–pad evaporative cooler that maintained an indoor air temperature of 20°C and an indoor relative humidity of 70%. Vala et al. [21] carried out a validation of the evaporative cooling system using CFD analysis and developed a mathematical model for predicting temperature, velocity, and humidity distribution. The model results and experimental results were similar.

An increase in average temperature leads to a corresponding decrease in relative humidity that affects the quality and shelf life of fruits and vegetables. In Kenya, about 25–45% of total fruit and vegetable production perishes due to inappropriate storage facilities. This is particularly alarming amongst rural farmers. In recent years, charcoal coolers have gained traction in Kenya's storage. However, charcoal coolers are the major source of greenhouse gas emissions. Therefore, a clean and low-cost evaporative cooling system was explored as an alternative to charcoal coolers for postharvest preservation. The primary objective of this study was to evaluate the performance of the evaporative cooling system with energy savings and thermal control in storage space using different cooling methods and to develop a Computational Fluid Dynamics (CFD) model to predict storage temperature. The conceptual examination of an evaporative cooling chamber with heat and mass transfer laws, coupled with CFD Therefore, conceptual examination of an evaporative cooler is vital for enlightening heat and mass transfer laws and forecasting outputs under various circumstances for numerical simulation [22]. The simulation of any fluid problem that can be solved numerically is possible with computational fluid dynamics. However, this simulation process is segmented into three primary stages: preprocessing, solving, and post processing [19], [23], [24], [25].

## II. Materials and Methods

### *A. Experimental setup*

A storage chamber fabricated at the Agricultural and Biosystems Engineering Department, School of Biosystems and Environmental Engineering, College of Engineering and Technology, Jomo Kenyatta University of Agriculture and Technology (JKUAT), Kenya, was used for this research. JKUAT is located in Juja, Kiambu County, Kenya, and has an annual average temperature of 19.6 $^{O}$C and an annual average There was 799 mm of rain. The geographical coordinates for JKUAT are a longitude of 37 $^{O}$ 01' East and a latitude of 1$^{O}$ 11' South with an elevation of 1550m above sea level [26]. The storage chamber is presented in Fig. 1 below.

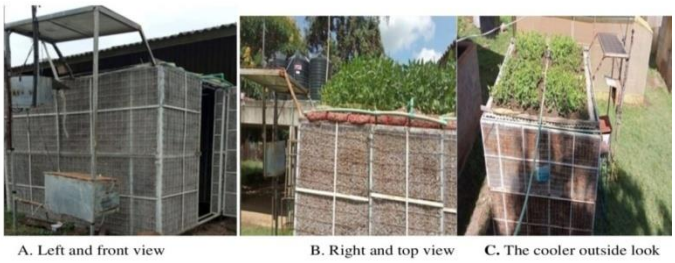


Figure 1. Photographic views of the evaporative cooling system at JKUAT

The evaporative cooling chamber was rectangular with a wider surface area for the circulation of air, as shown in Fig. 2 below. The cooler had a reservoir to retain water and two fans to support convective cooling. The top was covered with a corrugated iron sheet holding a layer of soil for plant growth. The internal and external walls of the cooling chamber were made of pumice. The geometrical dimensions of the cooler were 2.7m x 2.7m x 2m for length, breadth, and height, respectively. The pumice wall had a uniform thickness of 0.15m and the door was made with pumice of the same thickness.

The main frame of the cooler was made with iron poles and supported with wire mesh (0.024 mm) to hold the pumice. On top of the corrugated iron was topsoil, and cowpeas were planted to support cooling through evapotranspiration. There were two 12V fans with seven blades each mounted on the floor of the cooler that blew air upwards. Each fan had a swept depth diameter of 0.0012m. The purpose of these fans was to accelerate convective cooling. Below these fans was a reservoir to collect water and prevent water splash, which was later pumped back to the overhead thanks. There were three overhead tanks used through necessary piping to supply water for evaporative cooling through the wall of the storage chamber. A solar-powered electric pump was used to lift the water from the reservoir back into the overhead tanks while water passing through the gates was drained back into the reservoir. The pad (pumice) was water through a PVC pipe (0.0127 m) connected to three tanks, each with a storage capacity of 0.1 m3. These tanks were 2.5m above the ground.

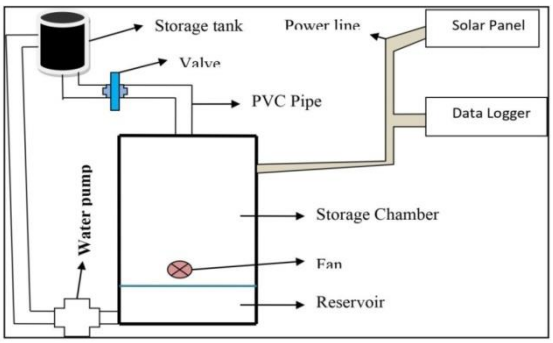


Figure 2. A two-dimensional model representation of the cooling system

The design of the front, rear, left and right sides were determined using Eq.1.

$$A_f = A_{re} = A_l = A_{ri} = H_C * L_C \quad (1)$$

where,

*$A_f$ is front side area ($m^2$), $A_{re}$ is real side area ($m^2$), $A_l$ is lift side area ($m^2$), $A_{ri}$ is right side area ($m^2$), $H_C$ is height of cooler (m) and $L_C$ is length of cooler (m).*

The design of the top and floor were done using Eq. 2.

$$A_t = A_{fl} = L_C * W_C \quad (2)$$

where,

$A_t$ is top area ($m^2$); $A_{fl}$ is floor area ($m^2$);and $W_C$ is width (m).

The volume/capacity was calculated using Eq. 3.

$$V_C = L_{Ca} * W_{Ca} * H_{Ca} \quad (3)$$

where,

*Vca is volume capacity ($m^3$); Lca is length capacity (m); Wca is width capacity (m); and Hca is height capacity (m)*

The floor fans capacity was calculated using Eq. 4 [27].

$$F_{capacity} = A_{floor} * (0.004 m^3 s^{-1}) \quad (4)$$

The installed floor fans and water pump had the following specifications: a voltage rating of 12V, a current of 0.15A, and a power rating of 1.8W. These specifications were considered in selecting the solar power for the continuous function of the fans and water pump. The solar panel selected had the following specifications: voltage of 17.6V, current of 7.1A, and power of 125W.

### *B. Data collection*

The data was collected using an Arduino SD card data logger designed and installed outside the storage chamber. It was connected to 10 DHT11 sensors that measured temperature and relative humidity (9 inside and 1 outside), with an accuracy of ± 2% and ± 5% respectively. The setup of the data collection points are shown in Fig. 3 below.

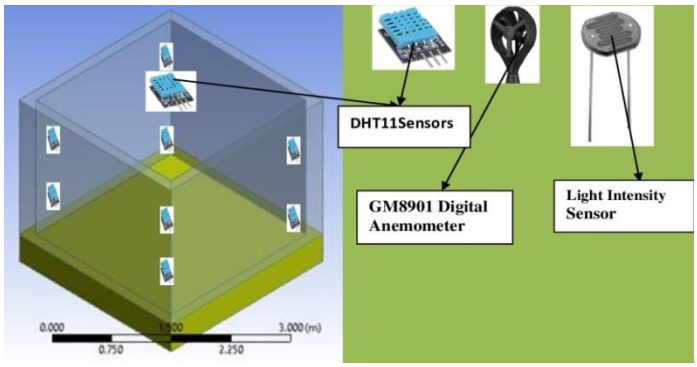


Figure 3. Data collection points for both ambient and storage chamber

Of the nine sensors inside the cooler, one was placed in the middle of the cooler at 10cm (y-direction) from the corrugated iron sheet ceiling, 120cm (x-direction) from the walls, and 190cm (z-direction) from the floor. Four were placed at the lower end corners of the cooler at 12cm (x-direction) from the wall, 145cm (y-direction) from the corrugated iron sheet ceiling, and 55cm (z-direction) from the floor; while the other four were placed at the upper-end corners of the cooler at 12cm (x-direction) from the walls, 50cm (y-direction) from the ceiling, and 150cm (z-direction) from the floor. On the outside, one DHT11 sensor measured ambient relative humidity and ambient temperature, a digital anemometer (GM8901, Qingdao) measured the outside wind speed up to 45m/s with an error of ± 3%; and a light intensity sensor (LDR, Shenzhen) with an operation temperature of-30 to + 70 $^{o}$C measured solar radiation (all 2.75m above the ground); were connected to a general purpose data logger. The GM8901 Digital Anemometer and Light Intensity Sensor (LDR) were calibrated using a Cr1000 data logger. The data logger automatically recorded temperature, relative humidity, solar intensity, and wind speed every 30 seconds, averaging every 30 minutes.

The data was collected from February 18 to April 6, 2020, at no charge to evaluate the performance of the chamber. In the first case, the cooler was not subjected to any form of cooling when data was collected for seven days from 8:00 am to 6:00 pm, generating a total data sample of 3,234 (DHT11: 1,470 for both relative humidity and temperature; GM8901 Digital Anemometer: 147 wind speed samples; and Light Intensity Sensor (LDR): 147 solar radiation samples). This setup and duration were followed for convective cooling only

and transpiration only, thereby recording 3,234 samples each. For evaporative cooling only, data was collected for eight days, and a total of 3,696 samples were recorded. Finally, convective, evaporative, and evaporative cooling were operated as a single system for eleven days and recorded total data samples of 5,082.

### C. Data analysis

The data was analyzed using student t-test, ANOVA, regression, and Python for average daily values. The data collected from the experimental setup and model-generated data were analyzed statistically using a student t-test and regression using PYTHON programming. Different methods were used to evaluate the performance of the storage chamber and the Computational Fluid Dynamics model.

#### 1) Student t-test

A student t-test is a form of statistical test used to compare the mean of two groups. The t-test was used to determine whether the experimental data is different from the model data and if the data collection process affects the population of interest. Equation 5 was used to calculate the t-value.

$$t = \frac{\bar{x}_1 - \bar{x}_2}{\sqrt{\left[s^2\left(\frac{1}{n_1} + \frac{1}{n_2}\right)\right]}} \quad (5)$$

where;

*t is the student's t-value*
*$X_1$ and $X_2$ are the mean of the two groups being compared*
*$S^2$ is the pooled standard error of the two groups and*
*$n_1$ and $n_2$ are the number of observations in each of the groups.*

#### 2) Regression analysis

Regression analysis is a statistical tool used to predict dependent variables with the help of one or more independent variables. Regression analysis was used to determine the relationship between experimental and model data. The relationship between the dependent and independent variables was calculated from Eq. 6.

$$Y = a + bX + E \quad (6)$$

where;

*Y is the dependent variable*
*a is the intercept*
*b is the slope*
*X is the independent variable and*
*E is the residual value*

The above equation tries to find the best fit line for the dependent variable with the help of the independent variables. Therefore, this regression analysis equation is the same as the equation of a line, which is written as:

$$y = MX + b \quad \mathbf{(7)}$$

where;

*y is the dependent variable of the regression equation*
*M is the slope of the regression equation*
*X is the dependent variable of the regression equation*
*b is the constant of the equation*

#### 3) Python programming

Both the t-test and regression statistical tools were implemented through python programming. The necessary models were imported into Anaconda for analysis. Some of the models imported into Python Anaconda for the statistical analysis were Math, Pandas, Numpy, Matplotlib.pyplot, sklearn.metrics, and Logistic Regression. Additional statistical analyses were carried out to analyze the data, which included: correlation coefficient (R), coefficient of determination (R2), mean square error (MSE), root mean square error (RMSE), mean relative error (MRE), mean absolute error (MAE), and mean absolute percent error (MAPE). The equations that were used for calculating R, R2, MSE, RMSE, MRE, MAE, and MAPE are presented below.

$$R = \frac{n(\sum xy) - (\sum x)(\sum y)}{\sqrt{[n(\sum x^2) - (\sum x)^2][n(\sum y^2) - (\sum y)^2]}} \quad (8)$$

$$R^2 = 1 - \frac{\sum_i e_i^2}{\sum_i (y_i - \bar{y})^2} \quad (9)$$

$$MSE = \frac{1}{n}\sum_{t=i}^{n} e_t^2 \quad (10)$$

$$RMSE = \sqrt{\frac{1}{n}\sum_{t=i}^{n} e_t^2} \quad (11)$$

$$MRE = \frac{1}{n}\sum_{t=i}^{n} \left|\frac{y_i - \hat{y}}{y_i}\right| \quad (12)$$

$$MAE = \frac{1}{n}\sum_{t=1}^{n} |e_t| \quad (13)$$

$$MAPE = \frac{100\%}{n}\sum_{t=i}^{n} \left|\frac{e_t}{y_t}\right| \quad (14)$$

### D. Computational Fluid Dynamics Modeling

A three-dimensional (3-D) CFD model was used to simulate temperature inside the storage chamber and was validated by comparing data obtained from the storage chamber with the modeled result. The case study that was used to validate the model was the evaporative cooling system at no-load conditions. The mode domain was discretized using tetrahedral element meshing, and the Richardson extrapolation method was used to evaluate the level of grid independence [28]. The Ansys FLUENT 2019R2 (ANSYS, Canonsburg, PA, USA) was used for the simulation. FLUENT uses advanced technology with algebraic multi-grid solvers with effective parallelization and quick simulation [29]. The SIMPLE discretization approach was used for the coupling of the porous media pressure-velocity and second-order upwind discretization was applied for the momentum, specific dissipation rate, and energy computation. A steady state simulation was performed to evaluate the air temperature.

#### 1) Numerical simulation

The equations of fluid flow and heat transfer are mathematical manipulations of the conservation laws of fluid mechanics. These equations were used to develop a numerical model that was used to predict the air temperature within an evaporative cooling system. These fundamental equations are:

$$\frac{\partial \rho}{\partial t} + \frac{\partial \rho u_i}{\partial x_i} = 0 \quad (1)$$

$$\frac{\partial \rho T}{\partial t} + \frac{\partial \rho T u_j}{\partial x_j} = \frac{\partial}{cp\, \partial x_j}\left[K \frac{\partial T}{\partial x_j}\right] \quad (2)$$

$$\frac{\partial \rho u_i}{\partial t} + \frac{\partial \rho u_i u_j}{\partial x_j} = -\frac{\partial \rho}{\partial x_i} + \frac{\partial}{\partial x_j}[u\left(\frac{\partial u_i}{\partial x_j} + \frac{\partial u_j}{\partial x_i}\right)] \quad (3)$$

where:

*ρ, t, μ, P, k, T, Cp, u, represent the density (kg.m$^{-3}$), time (s), dynamic viscosity (kg.m$^{-1}$.s$^{-1}$), pressure (Pa), thermal conductivity (W.m$^{-1}$.$^{o}$C$^{-1}$), temperature ($^{o}$C), specific heat capacity (J.kg$^{-1}$.$^{o}$C$^{-1}$), and velocity (m.s$^{-1}$), respectively.*

Six CFD turbulence models were tested to determine their suitability for predicting temperature. The tested models include Standard k-**ε**, Realizable k-£, RNG k-£, seven equations Reynolds stress model, Shear Stress Transport (SST) k-ω and standard k-ω model. It has been revealed in open pieces of literature that the SST k-ω model is more accurate than k-£ and k- ω models for cold storage simulation [23], [21], [22], [30]. The SST k-ω turbulence model is defined by transport equations [31].

$$\frac{\partial}{\partial t}(\rho k) + \frac{\partial}{\partial x_i}(\rho k u_i) = \frac{\partial}{\partial x_j}\left\{\Gamma_k \frac{\partial k}{\partial x_j}\right\} + \tilde{G_k} - Y_k + S_k \quad (4)$$

$$\frac{\partial}{\partial t}(\rho \omega) + \frac{\partial}{\partial x_j}(\rho \omega u_j) = \frac{\partial}{\partial x_j}\left\{\Gamma_\omega \frac{\partial \omega}{\partial x_j}\right\} + G_\omega - Y_\omega + D_\omega + S_\omega \quad (5)$$

$$\tilde{G_k} = \min(G_k, 10\rho\beta * k\omega \quad (6)$$

$$G_\omega = \frac{\alpha}{v_t}\tilde{G_k} \quad (7)$$

$$\Gamma_k = \mu + \frac{\mu_t}{\sigma_k} \quad (8)$$

$$\Gamma_\omega = \mu + \frac{\mu_t}{\sigma_\omega} \quad (9)$$

where;

*$G_k$, $G_\omega$, $\alpha$, $D_\omega$, and $\mu_t$ are turbulence kinetic energy (m$^2$.s$^{-2}$), the generation of ω, low-Reynolds number correction, the cross-diffusion term (m$^2$.s$^{-1}$), and the turbulent viscosity (kg.m$^{-1}$.s$^{-1}$), respectively. $\Gamma_k$ and $\Gamma_\omega$ = effective diffusivity of k and ω respectively. $Y_k$ and $Y_\omega$ = dissipation of k and ω due to turbulence. $S_k$ and $S_\omega$ = source terms. $\sigma_k$ and $\sigma\omega$ = turbulent Prandtl numbers, and $\mu_t$ = turbulent viscosity (kg.m$^{-1}$.s$^{-1}$)*

The simulation was implemented with a pressure-based solution algorithm, solved using second-order upwind energy and momentum discretization, a SIMPLE pressure-velocity coupling, and "Body Force" weighted pressure discretization. The second-order upwind scheme uses a multidimensional linear rebuilding method to solve for quantities at cell faces, and the body-force-weighted scheme calculates face pressure by assuming the normal gradient between pressure and body force as constant. The SIMPLE pressure-velocity coupling uses a relationship between velocity and pressure corrections to enforce mass conservation and pressure field [31], [32]. The air inside the storage chamber was considered incompressible and its density varied according to ideal gas law due to the buoyancy effect. Other thermal properties (specific heat, thermal conductivity, and viscosity) were maintained constant.

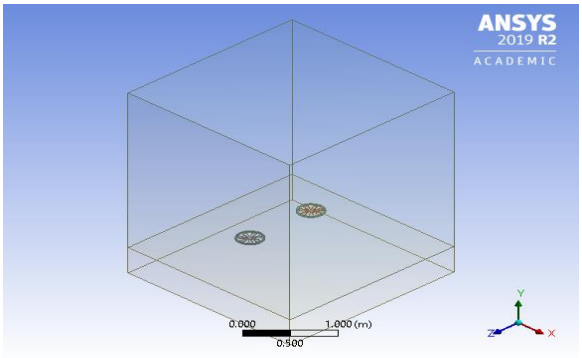


Figure 4. CFD model of the evaporative cooler

*2) Model meshing*

The computational domain was discretized with an automatic mesh method using an in-built ANSYS design modeler meshing algorithm set to orthogonal quality and maximum skewness of 0.9. The mesh density was gradually refined, and the final mesh size consisted of 501,358 elements and 389,244 nodes. The minimum and maximum element sizes were set at 0.05m and 0.1m, respectively. Five inflation layers were employed along the wall surfaces. The first element was 0.05m, and the growth ratio was 1.2, with a maximum element size of 0.1m. The mesh independence was done by testing the validity and quality of discretization.

This test was to ensure that the solution is accurate regardless of the mesh size. To conduct a grid independence test, the solutions must be obtained with multiple mesh sizes and observed in their outcomes. Six different mesh sizes were tested for temperature and mass flow rate with the first initial solution ran with 0.1m minimum and 0.2m maximum, which gave 97,638 elements and 25,289 nodes; then refined for the next solutions to 0.09m, 0.07m, 0.06m, 0.05m, and 0.04m for minimum element sizes. Table 1 shows the simulation results for different mesh sizes used for the independent test before selecting 0.05m. The simulation time was 4 to 8 hours, with over 3000 iterations before the solution converged on an HP Window 10 Pro LAPTOP-SCJFUG9 with a processing capacity of AMD A8-7410 APU 2.20 GHz and a 64-bit operating system, X64-based HP Processor.

Table I: Mesh independence test

| Minimum element size (m) | Maximum element size (m) | Number of nodes $10^3$ | Number of elements $10^3$ | Mass (g/s) | Temperature ($^{o}$C) |
|---|---|---|---|---|---|
| 0.1 | 0.2 | 25 | 97 | 8.229 | 19.76 |
| 0.09 | 0.16 | 30 | 119 | 8.230 | 19.74 |
| 0.07 | 0.14 | 41 | 161 | 8.232 | 19.70 |
| 0.06 | 0.12 | 58 | 232 | 8.236 | 19.68 |
| 0.05 | 0.1 | 89 | 361 | 8.239 | 19.66 |
| 0.04 | 0.08 | 159 | 634 | 8.239 | 19.66 |

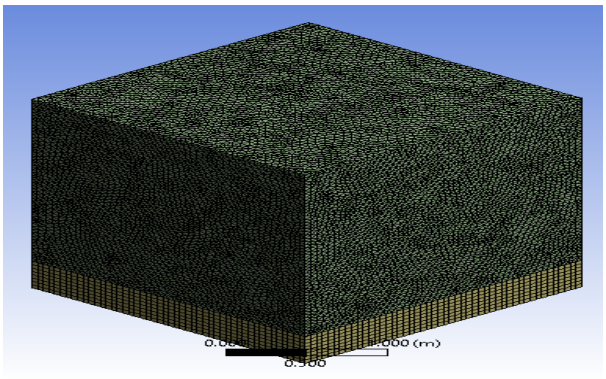

Figure 4. Mesh section of the computational model

*3) Boundary conditions*

The thermal and momentum boundary conditions were considered based on the experimental results for temperature and wind [31], [33]. To simplify the complexity of the simulation, some necessary assumptions were made as follows:

1. The system was in a steady-state condition.
2. The flow was internal, incompressible, and multiphase.
3. The thermo-physical properties of materials are independent of temperature.

*4) Convergence criteria*

In some cases, only two conditions of quantity imbalances and stability of monitored quantities can indicate the convergence even if the condition of residuals is not completely satisfied. However, when the imbalances or monitor conditions are not satisfied, then the solution is not yet converged. The following convergence criteria were used for this study:

1. The overall mass and energy conservation was achieved with mass and energy imbalances of less than one percent (1%). These imbalances measure global mass and energy conservation.
2. The residuals for the momentum and continuity equations dropped to less than 10-3 and less than 10-6 for the energy equation.
3. The quantities of interest reached stability as indicated by the solution monitors, such as the storage outlet temperature and mass flow rate. A stable monitor is when the simulation results no longer change with further iteration.

## E. Post-processing

The result from the modeled storage chamber (using the temperature distribution method) shows that the storage temperature varied from 18.37 ºC (291.52 ºK) to 24.29 ºC (297.44 ºK). This result shows that the model output is much lower than the ambient temperature, and the predicted temperature is in close agreement with the storage temperature.

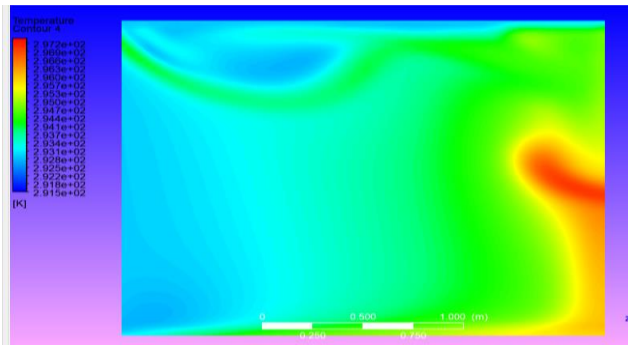

**Figure 5 Model temperature profile**

# III. RESULTS AND DISCUSSION

## A. Fruits and vegetable storage

Improved vegetable storage is needed where the ambient temperature is higher and the relative humidity is lower than the ideal storage conditions for a specific vegetable. When assessing the potential benefits of a storage system for a given product, it is essential to consider how the storage conditions are achieved within the system. The ideal storage conditions for tomatoes are between 18 °C and 22 °C and the relative humidity is between 80% and 95% [34]. In tropical countries, it is seemingly difficult to obtain these conditions, and therefore a considerable quantity of harvested tomatoes end up as waste. This is consistent with the claim that the quality of tomatoes is compromised when exposed to high temperatures and low relative humidity. Storage can extend the shelf life of fruits and vegetables, and extend the processing season and product availability beyond their harvesting season [21].

## B. Temperature predictions

This subsection presents the results from the modeled storage chamber. The result shows that the storage space temperature varied from 18.37 ºC (291.52 ºK) to 24.29 ºC (297.44 ºK) depending on the probe location and time. This result shows that the model output is much lower than the ambient temperature and with an acceptable prediction of the storage temperature. Figure 6 shows the time-average contours of temperature distribution across the storage space. The time average variation of temperature was mainly because of different boundary conditions that were considered during the model setup. The materials of paramount concern were given boundary conditions based on experimental data, while others were set at no-slip conditions. Because of the different material surfaces separating the storage space from either side of the cooler, these variations were unavoidable. The seven equation Reynolds stress model had a better prediction than the others; however, there was a significant increase in computational time. Several computational errors were noticed in k-£ models, while the standard k-ω model was less accurate compared to the SST k-ω model.

The SST k-ω turbulence model is a two-equation eddy-viscosity model that was developed to effectively simulate near-wall regions of complex geometries, determined turbulent length, and time-scale solutions [30]. The SST k-ω turbulence model combines the k-ω formulas for inner parts of the boundary layer and the SST switches the k-ε behavior in the free-stream, making it appropriate for Low-Reynolds turbulence modeling without extra damping functions.

*1) Model validation*

The model was validated by comparing experimental temperatures with the predicted temperatures, including measurement uncertainty at probe locations as shown in Table 2. In general, the model shows a good level of prediction for air temperature distribution in space.

Table. II Experimental temperature and predicted temperature at 30 minutes interval from 8am to 6pm

| Time | Amb. Temp. | **Average Storage temperature** | | | | | Pred. Temp. |
|---|---|---|---|---|---|---|---|
| | | Case 1 | Case 2 | Case 3 | Case 4 | Case 4 | |
| 08:00 | 19.37 | 18.64 | 18.37 | 18.91 | 18.6 | 18.44 | 18.37 |
| 08:30 | 21.89 | 18.87 | 18.8 | 18.95 | 18.75 | 18.48 | 18.67 |
| 09:00 | 26.15 | 19.28 | 19.17 | 19.03 | 19 | 18.66 | 18.96 |
| 09:30 | 29.69 | 20.07 | 19.69 | 19.24 | 19.43 | 18.9 | 19.26 |
| 10:00 | 34.11 | 20.55 | 20.41 | 19.6 | 19.81 | 19.33 | 20.55 |
| 10:30 | 37.63 | 21.48 | 21.36 | 20.11 | 20.62 | 20 | 20.85 |
| 11:00 | 40.24 | 22.37 | 22.31 | 20.56 | 21.27 | 20.58 | 21.15 |
| 11:30 | 41.01 | 23.12 | 23.2 | 20.94 | 21.86 | 20.91 | 21.44 |
| 12:00 | 43.21 | 23.46 | 23.84 | 21.4 | 22.4 | 21.29 | 22.01 |
| 12:30 | 41.41 | 23.96 | 24.12 | 21.77 | 22.62 | 21.54 | 22.52 |
| 13:00 | 42.5 | 24.37 | 24.9 | 22 | 22.8 | 21.76 | 22.89 |
| 13:30 | 41.42 | 24.82 | 24.96 | 22.17 | 23.07 | 21.96 | 23.1 |
| 14:00 | 42.28 | 25.34 | 25.26 | 22.36 | 23.31 | 22.1 | 23.61 |
| 14:30 | 42.04 | 25.84 | 25.49 | 22.48 | 23.62 | 22.54 | 22.75 |
| 15:00 | 40.95 | 26.35 | 25.29 | 22.76 | 23.84 | 22.78 | 23.14 |
| 15:30 | 40.09 | 26.73 | 25.43 | 23.04 | 23.94 | 22.97 | 22.93 |
| 16:00 | 36.36 | 26.58 | 26.06 | 22.93 | 23.8 | 22.99 | 22.51 |
| 16:30 | 31.21 | 26.11 | 24.7 | 22.82 | 23.51 | 22.79 | 22.57 |
| 17:00 | 28.93 | 25.54 | 24.36 | 22.46 | 22.99 | 22.59 | 22.9 |
| 17:30 | 27.89 | 24.94 | 23.95 | 22.06 | 22.54 | 22.36 | 21.63 |
| 18:00 | 25.24 | 24.28 | 23.45 | 21.66 | 22.1 | 22.08 | 21.33 |

*C. Performance evaluation of the storage system*

The performance of the cooling system was conducted by comparing ambient conditions to storage conditions at the time of day. The data obtained from the sensors shows that when ambient relative humidity is low ( 35%) and ambient temperature is high (> 26 $^{O}$C), the storage temperature was lowered by 8–13 $^{O}$C and relative humidity was kept above 86%. These results are consistent with the principle of evaporation (the cooling effect is reduced with increasing ambient humidity). The evaporative cooling technology provides greater benefits along the fruit and vegetable postharvest value chain for farmers, traders, and consumers. These benefits are robust if the postharvest loss is due to high temperatures and low relative humidity exposure. Some vegetables that are particularly susceptible to these conditions are tomatoes, okra, eggplants, and leafy greens. In general, evaporative coolers are best suited to providing these benefits in dry and hot climates.

*D. Storage chamber with a bare roof and no cooling*

The storage temperature and relative humidity with no cooling technology applied to the cooler ranged from 18.64 to 26.73 $^{O}$C (daily average 23.46 $^{O}$C) and 68.75 to 72.91% (daily average 70.78%) for seven days, respectively. The average ambient temperature and relative humidity during the same period were 34.93 $^{O}$C and 28.34%, respectively. The storage chamber was able to reduce the temperature by an average of 11.47 $^{O}$C while the relative humidity increased by 42.44%. The cooling efficiency was 83%. Comparing storage temperature to model predicted temperature resulted in the following findings: coefficient of determination (R2) = 0.88, mean square error (MSE) = 5.14, root mean square error (RMSE) = 2.34, and correlation = 0.86.

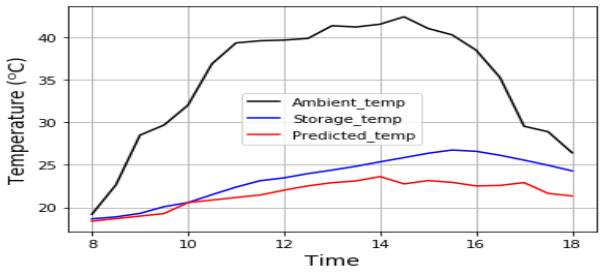


Figure 6. Ambient temperature, storage temperature, and model predicted temperature for no cooling

*E. Convective cooling*

The temperature and relative humidity of the application of convective cooling technology for seven days ranged from 18.37 to 26.06 $^{O}$C (daily average 23.1 $^{O}$C) and 71.31 to 74.39% (daily average 72.52%) respectively. The average ambient temperature and relative humidity for the same period were 34.58 $^{O}$C and 28.46% respectively. The storage chamber was able to reduce the temperature by an average of 11.48 $^{O}$C and increased relative humidity by 44.06%. The cooling efficiency was 85%. Comparing storage temperature to model predicted temperature resulted in the following findings: R2 = 0.89, MSE = 3.3, RMSE = 1.8 and correlation = 0.94.

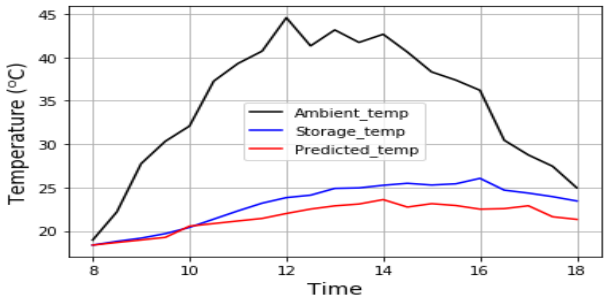


**Figure 7.** Ambient temperature, storage temperature, and model predicted temperature for convective cooling

*F. Evaporative cooling*

The storage temperature and relative humidity with evaporative cooling technology from 8 AM to 6 PM for eight days ranged from 18.91 to 23.04 $^{O}$C (daily average 21.29 $^{O}$C) and 91.78 to 92.94% (daily average 92.78%) respectively. The

average ambient temperature and relative humidity for the same period were 35.06 $^{O}$C and 28.09% respectively. The storage chamber was able to reduce the temperature by an average of 13.12 $^{O}$C and increased the relative humidity by 64.69%. The cooling efficiency was 98.6%. Comparing storage temperature to model predicted temperature resulted in the following findings: R2 = 0.89, MSE = 0.36, RMSE = 0.6 and correlation = 0.9.

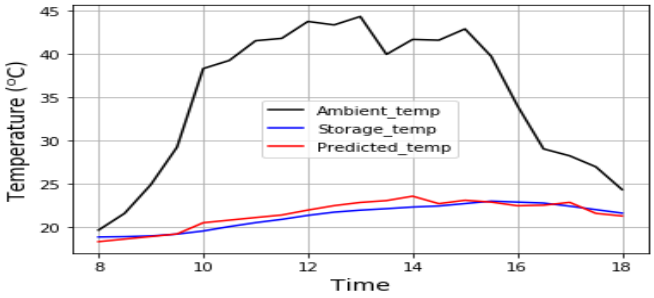


Figure 8. Ambient temperature, storage temperature, and model predicted temperature for evaporative cooling

### G. *Evapotranspiration cooling*

The storage temperature and humidity with the evapotranspiration cooling technology from 8 AM to 6 PM for seven days ranged from 18.6 to 23.94 $^{O}$C (daily average 21.89 $^{O}$C) and 74.16 to 76.87% (daily average 75.61%) respectively. The average ambient temperature and relative humidities were 35.14 $^{O}$C and 27.99% respectively. The storage chamber was able to reduce the temperature by an average of 13.25 $^{O}$C and increased the relative humidity by 47.62%. The cooling efficiency was 94%. The data collection started nine days after the cowpeas were planted on top of the cooler, at wish time the crop's average height was 0.3m and by the end of the data collection, the crops' average height was 0.8m. Comparing storage temperature to model predicted temperature resulted in the following findings: R2 = 0.9, MSE = 0.35, RMSE = 0.6 and correlation = 0.9.

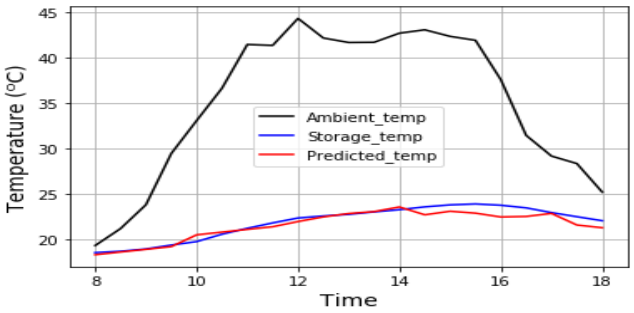


**Figure 9.** Ambient temperature, storage temperature, and model predicted temperature for evapotranspiration cooling

### H. *Combined cooling technologies*

The final performance test for the no-load storage chamber was conducted as a single system comprising the previously discuss cooling methods. The temperature and relative humidity for eleven days from 8 am to 6 pm ranged from 18.44 to 22.99 $^{O}$C ( daily average 21.19 $^{O}$C) and 92.55 to 94.88% (daily average 93.95%) respectively. The temperature was lowered by 13.74 $^{O}$C, while relative humidity was increased by 65.8%. The ambient average values for temperature and relative were 34.9 $^{O}$C and 28.13% respectively. The cooling efficiency of the system was 99%. Figures 11 and 12 show the comparison of ambient temperature to storage temperature, and ambient relative humidity to storage relative humidity respectively. Comparing storage temperature to model predicted temperature resulted in the following findings: R2 = 0.85, MSE = 0.5, RMSE = 0.7 and correlation = 0.8.

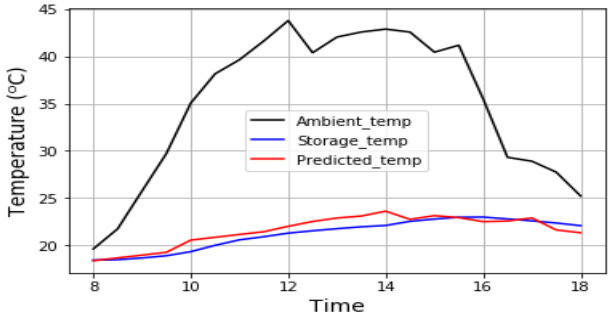


Figure 10. Ambient temperature, storage temperature, and model predicted temperature for combined cooling

### I. *Storage optimization*

The result shows the pad thickness of 0.2m improved the cooling efficiency by 2% above the current design. Table 5.3 presents the optimized evaporative cooling chamber based on cooling efficiency using the CFD model. The optimum point based on the single variable (pad thickness) is 200 mm. The dependent variable was the predicted temperature; all other parameters were constant (water flow rate, velocity, and ambient temperature).

Table III. Storage optimization based on pad thickness

| No | Pad thickness (mm) | Flow rate (l/min) | Air velocity (m/s) | Amb. Temp. ($^{O}$C) | Pred. Temp ($^{O}$C) | Efficiency (%) |
|---|---|---|---|---|---|---|
| 1 | 50 | 1.75 | 0.6 | 34.93 | 23.1 | 71 |
| 2 | 100 | 1.75 | 0.6 | 34.93 | 21.89 | 80 |
| 3 | 150 | 1.75 | 0.6 | 34.93 | 21.19 | 83 |
| 4 | 200 | 1.75 | 0.6 | 34.93 | 20.29 | 85 |
| 5 | 250 | 1.75 | 0.6 | 34.93 | 20.29 | 85 |

### *J. Optimum pumice pad thickness*

Figure 12 shows the changes in temperature inside the storage and the change in pad thickness. The optimum point on the graph occurred at a pad thickness of 200 mm, which resulted in a storage temperature of 20.29 °C. The model predicted that when the pad thickness was increased to 250 mm, the model predicted the same as the 200 mm pad thickness. Therefore, the researcher's conclusion on the optimum pad thickness using the single variable optimization method is 200 mm.

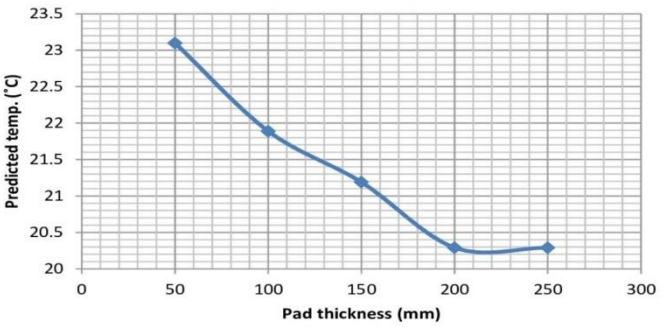


Figure 12. The plot showing the optimum pad thickness

## IV. Conclusion

Postharvest storage difficulties facing local farmers in tropical countries like Kenya can be curtailed through evaporative cooling technology. Adequate and appropriate storage structures can increase the shelf-life of fruits and vegetables, thereby increasing growers' earnings, produce availability, and spoilage. Temperature and relative humidity control are critical in providing fresh produce safety, prolonging shelf-life, and maintaining quality. Accordingly, tomato shelf-life can be extended for up to 15–25 days when stored in this cooling chamber. The study provides useful guidelines for the design of an evaporative cooling system with efficient energy savings for the storage of fruits and vegetables. The concluding remarks are summarized as follows:

a. contributed to the knowledge of temperature and relative humidity distribution within the chamber with alternative influences on the system. The monitoring of the cooling chamber provided evidence of the temperature and relative humidity distribution.

b. The uniformly lowest temperatures and highest relative humidity distribution were reported during evaporative and combined cooling. The experimental data was used to develop and simulate the temperature in the storage chamber.

c. Storage chambers constructed with pumice provide a good storage environment to preserve fruits and vegetables.

d. The study shows that with no cooling, the temperature was reduced by 11.47 $^{O}$C; while relative humidity was increased by 42.44%. The cooling efficiency of the pumice was 83%. The storage temperature was further lower by 0.36, 2.17, 1.57, and 2.27 $^{O}$C for convection, evaporation, transpiration, and combined technologies; while relative humidity was increased by 1.74, 22, 4.83, and 23.17% respectively. The cooling efficiency was increased from 83% to 85, 98.6, 94, and 99% for convection, evaporation, transpiration, and combined technologies, respectively.

## Acknowledgement

The author appreciates the Jomo Kenyatta University of Agriculture and Technology for allowing me to use their facilities for this project.

Additionally, I acknowledge the overwhelming support from the members of the staff of the Department of Environmental and Biosystems Engineering, University of Nairobi; and the Department of Agricultural and Biosystems Engineering, JKUAT.

I would like to express my very special gratitude to my family; Hawa Kumba Tumbay (mother), Setta Sia Tumbay (sister), and Dr. James K. Sowah Jr. (brother) for their unlimited support.

To my friends; Solo B. Gbayor, Trokon G. Smith, Amos M. Kollie, P. Sharbar Zayzay, and Joseph S. Bundoo; I say thank you for your moral and financial support.

To the Lofa County Community College, I remain grateful for granting me a study leave.

Finally, I am thankful to my postgraduate colleagues at the Department of Environmental and Biosystems Engineering, University of Nairobi.

May the sufficient Grace of our Lord Jesus Christ be with us all!

## References

[1] Rosegrant, M. W., Magalhaes, E., Valmonte-Santos, R. A., & Mason-D'Croz, D. (2018) Returns to investment in reducing postharvest food losses and increasing agricultural productivity growth Prioritizing development: A cost benefit analysis of the United Nations' sustainable development goals, 322-338

[2] Kituu, G. M., Korir, M. K., Mutwiwa, U., & Sila, D. N. (2014). Development of a computer model simulation for predicting the performance of a near infrared reflecting charcoal cooler for on farm storage of mangoes

[3] Kitinoja, L., & Kader, A. A. (2015) Measuring postharvest losses of fresh fruits and vegetables in developing countries Postharvest Education Foundation, 1-26

[4] Kipruto, K. M. (2017). Effect of near infrared reflection and evaporative cooling on quality of mangoes *Agricultural Engineering International: CIGR Journal*, *19*(1), 162-168

[5] Singh, M. C., Yousuf, A., & Singh, J. P. (2016). Greenhouse microclimate modeling under cropped conditions-A review. *Res. Environ. Life Sci*, *9*, 1552-1557.

[6] Duan, L. B., Zhao, X. R., Liu, J. M., Geng, W. C., Xie, H. Y., & Sun, H. N. (2012). Effect of annealing ambient on the structural, optical and electrical properties of (Mg, Al)-codoped ZnO thin films. *Physica Scripta*, *85*(3), 035709.

[7] Sultan, M., Miyazaki, T., & Koyama, S. (2018) Optimization of adsorption isotherm types for desiccant air-conditioning applications. *Renewable Energy*, *121*, 441-450.

[8] James, A., &Zikankuba, V. (2017) Postharvest management of fruits and vegetable: A potential for reducing poverty, hidden hunger and malnutrition in sub-Sahara Africa. Cogent Food & Agriculture, 3(1), 1312052

[9] Roy, S. K., & Pal, R. K. (1989, September) A low cost zero energy cool chamber for short term storage of mango. In III International Mango Symposium 291 (pp. 519-524).

[10] Mordi, J. I., & Olorunda, A. O. (2003) Effect of evaporative cooler environment on the visual qualities and storage life of fresh tomatoes *Journal of food science and technology (Mysore)*, *40*(6), 587-591

[11] Kitinoja, L. (2013) Use of cold chains for reducing food losses in developing countries. Population, 6(1.23), 5-60Krishnakumar, K., & Goldberg, D. E. (1992) Control system optimization using genetic algorithms Journal of Guidance, Control, and Dynamics, 15(3), 735-740

[12] Manyozo, F. N., Ambuko, J., Hutchinson, M. J., & Kamanula, J. F. (2018). Effectiveness of evaporative cooling technologies to preserve the postharvest quality of tomato. *International Journal of Agronomy and Agricultural Research*, *13*, 114-127.

[13] Liu, H., Zhou, Q., Liu, Y., Wang, P., & Wang, D. (2015) Experimental study on cooling performance of air conditioning system with dual independent evaporative condenser International journal of refrigeration, 55, 85-92.

[14] Ambaw, A., Delele, M. A., Defraeye, T., Ho, Q. T., Opara, L. U., Nicolaï, B. M., & Verboven, P. (2013) The use of CFD to characterize and design post-harvest storage facilities: Past, present and future. Computers and Electronics in Agriculture, 93, 184-194.

[15] Sohani, A., Sayyaadi, H., & Hoseinpoori, S. (2016). Modeling and multi-objective optimization of an M-cycle cross-flow indirect evaporative cooler using the GMDH type neural network *International Journal of Refrigeration*, *69*, 186-204.

[16] Luo, Y., Yang, H., Lu, L., & Qi, R. (2014) A review of the mathematical models for predicting the heat and mass transfer process in the liquid desiccant dehumidifier Renewable and Sustainable Energy Reviews, 31, 587-599

[17] Montazeri, H., Blocken, B., & Hensen, J. L. M. (2015) Evaporative cooling by water spray systems: CFD simulation, experimental validation and sensitivity analysis. Building and environment, 83, 129-141

[18] Yanhua, L., Enli, L., Rahman, M. M., Yu, W., Jiaming, G., &Jie, Z. (2017). Numerical simulation of temperature and relative humidity in zero energy cool Chamber International Journal of Agricultural and Biological Engineering, 10(3), 185-193.

[19] Mishra, P., & Aharwal, K. R. (2018, August) A review on selection of turbulence model for CFD analysis of air flow within a cold storage In IOP Conference Series: Materials Science and Engineering (Vol. 402, No. 1, p. 012145) IOP Publishing

[20] Adarsh, S. S., & Jinu, A. (2017). *Development and testing of evaporative cooling box for naturally ventillated greenhouse* (Doctoral dissertation, Department of Soil and Water Conservation Engineering)

[21] Vala, K. V., Makwana, M., &Sagarika N. (2019) Validation of Evaporative Cooling System using CFD Analysis Int. J. Curr. Microbiol App. Sci, 8(3), 393-399

[22] She, X., Wu, J., Xu, H., Zhong, J., Wang, Y., Song, Y. &Vajtai, R. (2017) High Efficiency Photocatalytic Water Splitting Using 2D α-Fe2O3/g-C3N4 Z-Scheme Catalysts Advanced Energy Materials, 7(17), 1700025

[23] Tolesa, G. N. (2018). Modelling of micro-environment inside evaporatively and coolbot cooled stores using computational fluid dynamics models and changes in quality of stored tomatoes (Doctoral dissertation, University of KwaZulu-Natal Pietermaritzburg South Africa).

[24] Allen, R. G., Pereira, L. S., Raes, D., & Smith, M. (1998). Crop evapotranspiration-Guidelines for computing crop water requirements-FAO Irrigation and drainage paper 56. *Fao, Rome*, *300*(9), D05109.

[25] Hollender, J., Schymanski, E. L., Singer, H. P., & Ferguson, P. L. (2017). Nontarget screening with high resolution mass spectrometry in the environment: ready to go?.

[26] Sow, I., Murimi, E., & Mutwiwa, U. (2020). Evaporative Cooler Climate Prediction using Artificial Neural Network. *JOURNAL OF SUSTAINABLE RESEARCH IN ENGINEERING*, *5*(3), 113-127.

[27] Kumar, R., Chandra, S., Samsher, B. S., Kumar, R., & Kumar, A. A. (2018). Zero energy cool chamber for food commodities: Need of eco-friendly storage facility for farmers: A review. *Journal of Pharmacognosy and Phytochemistry*, *7*(5), 2293-2301

[28] Franke, J., & Frank, W. (2008) Application of generalized Richardson extrapolation to the computation of the flow across an asymmetric street intersection *Journal of Wind Engineering and Industrial Aerodynamics*, *96*(10-11), 1616-1628

[29] Kapilan, N., Gowda, M. M., & Manjunath, H. N. (2016) Computational Fluid Dynamics Analysis of an Evaporative Cooling System *Strojnícky časopis-Journal of Mechanical Engineering*, *66*(2), 117-124

[30] Ambaw, A., Bessemans, N., Gruyters, W., Gwanpua, S. G., Schenk, A., De Roeck, A & Nicolai, B. M. (2016). Analysis of the spatiotemporal temperature fluctuations inside an apple cool store in response to energy use concerns. International Journal of Refrigeration, 66, 156-168.

[31] Ansys, H. F. S. S. "High frequency electromagnetic field simulation." *Retrieved from* (2019)

[32] Menter, F. R. (1994). Two-equation eddy-viscosity turbulence models for engineering applications. *AIAA journal*, *32*(8), 1598-1605.

[33] Akdemir, S., Ozturk, S., Edis, F. O., & Bal, E. (2013). CFD Modelling of two different cold stores ambient factors. *IERI Procedia*, *5*, 28-40.

[34] Genanew, T. (2013) Effect of post harvest treatments on storage behavior and quality of tomato fruits *World Journal of Agricultural Sciences*, *9*(1), 29-37